Experimental results of a multimode monopile offshore wind turbine support structure subjected to steep and breaking irregular waves

Loup Suja-Thauvin
NTNU, Department of Marine Technology
Trondheim, Norway
loups@stud.ntnu.no

Jørgen R. Krokstad
NTNU, Department of Marine Technology
Trondheim, Norway

Erin E. Bachynski
NTNU, Department of Marine Technology
Trondheim, Norway

Erik-Jan de Ridder
MARIN
Wageningen, The Netherlands

We present experimental data from MARIN on a bottom-fixed offshore wind turbine mounted on a monopile in intermediate water depth subjected to severe irregular wave conditions. Two models are analysed: the first model is fully flexible and its 1st and 2nd eigenfrequencies and 1st mode shape are representative of those of a full-scale turbine. This model is used to study the structural response with special focus on ringing and response to breaking wave events. The second model is stiff and is used to analyse the hydrodynamic excitation loads, in particular the so-called secondary load cycle. The largest responses are registered when the second mode of the structure is triggered by a breaking wave on top of a ringing response. In such events, the quasi-static response accounts for between 40 and 50% of the total load, the 1st mode response between 30 and 40%, and the 2nd mode response up to 20%. A statistical analysis on the occurrences and characteristics of the secondary load cycle shows that this phenomenon is not directly linked to ringing.

Keywords: offshore wind turbine, monopile, ringing, slamming, modal decomposition, experimental hydrodynamics

1. Introduction

Over their lifetime, many bottom-fixed offshore wind turbines will encounter steep or breaking waves that might produce large structural responses. A number of offshore wind farms are planned or being developed in the North Sea, in water depths between 20 and 50 m (Ho et al., 2016). At these depths, interaction with the sea bottom enhances the wave nonlinearity, increasing the likelihood of breaking waves (Dalrymple and Dean, 1991). When designing the support structure of an offshore wind turbine for a specific site, the industry has to assess the maximum expected response that the structure will experience over its lifetime (so-called Ultimate Limit State (ULS) analysis, DNV, 2014a; DNV, 2014b; IEC, 2009).

Under ULS conditions, experiments have shown that the natural period of the structure can be suddenly excited by non-breaking waves whose fundamental period lies far from the structure's eigenperiod (Marthinsen et al., 1996; Stansberg et al., 1995;

Welch et al., 1999). This phenomenon, called 'ringing', is characterized by a fast build-up of transient resonant vibrations (only a few oscillations; Chaplin et al., 1997) and a much slower decay (Natvig and Teigen, 1993). In the case of a monopile type of support structure such as the one studied in this paper, ringing occurs during the passage of steep waves whose height is of the same order of magnitude as the diameter of the cylinder and whose fundamental period is around 3 times the natural period of the structure. Figure 1 shows an illustration of a ringing event. The bending moment has been filtered to show only the response of the first mode of the structure (this procedure is explained in section 4). After the passage of a very steep wave, the first mode gets suddenly excited and then decays slowly.

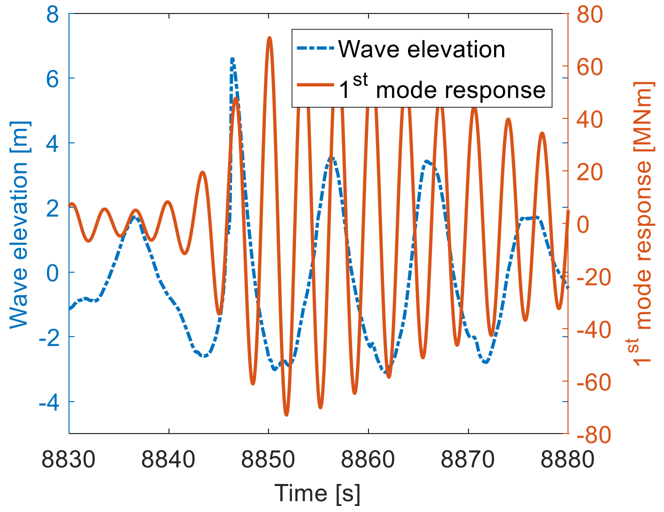

Figure 1. Illustration of a ringing event. A surface-piercing vertical cylinder is exposed to a steep wave, and the bending moment is measured at the sea bottom. The 1st mode is suddenly triggered and slowly decays, which is a typical characteristic of ringing events.

The ringing phenomenon started gaining attention in the 1990s when it was first observed on model tests of the Hutton and Heidrun TLP offshore oil and gas platforms, and then on the deep water concrete towers of the Draugen and Troll A platforms (Natvig and Teigen, 1993). Recently, the increase in size of offshore wind turbines combined with the limitation of the blade tip velocity has led to decreasing natural frequencies of the support structure down to a level where the 3rd harmonic of large waves (i.e. three times the fundamental frequency) coincides with the first structural natural frequency. This intensifies the risk of ringing response when subjected to extreme storms (see Suja-Thauvin et al., 2014). In addition to higher order hydrodynamic loads, breaking wave events have been a major concern for offshore structures. Both de Ridder et al. (2011) and Bredmose et al. (2013) carried out experiments on a bottom-fixed responding structure (as opposed to a stiff structure) whose characteristics were similar to those of an idling extra-large wind turbine (i.e. with the blades completely pitched to feather to limit the aerodynamic loading) and found that breaking waves could lead to extreme accelerations of the nacelle.

The main objective of this paper is to examine the process of maximum response of monopile offshore wind turbines under extreme stochastic sea states, in particular assessing the importance of the second mode of the structure and the characteristics of the measured excitation. In order to do so, we analyse data from experiments carried out in the Maritime Research Institute Netherlands (MARIN). The tests were performed within the project Wave Impact on Fixed structures (WiFi JIP). The characteristics of the model used for the experiment are those of an idling 4 MW bottom-fixed offshore wind turbine mounted on a monopile. These tests were performed with both a flexible and a stiff model in order to be able to measure the response and the excitation of the structure. Here, we focus on the measured excitation and response rather than on the wave kinematics. A correct understanding of the most important physical effects is an important first step in developing and validating engineering models which incorporate the relevant nonlinearities in the wave kinematics and in the wave-structure interaction.

In addition to the response analysis, we examine the phenomenon known as "secondary load cycle", or SLC, which appears as a rapid and high frequency increase of the excitation force, as Grue et al., (1993) described from their experiments. An occurrence of a SLC (sometime referred to as 'hydraulic jump') is highlighted in Figure 2. The SLC typically occurs about one quarter wave period after the main peak of the excitation force (Grue and Huseby, 2002) and lasts for about 15% of the wave period (Grue et al., 1993).

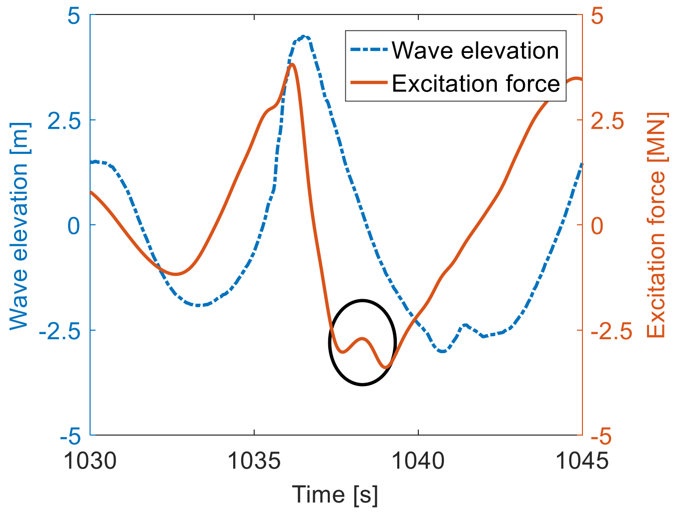

Figure 2. Occurrence of secondary load cycle, visible on the excitation force (circled in black).

Occurrences of SLCs have been extensively reported for steep waves in experiments in infinite water depths (see Chaplin et al., 1997; Grue et al., 1993; Grue and Huseby, 2002; Stansberg et al., 1995; Welch et al., 1999). Grue and Huseby (2002) also summarized the experimental data from those papers to establish a trend of occurrences of the SLC. One of their conclusions is that flow separation effects might reduce the likelihood of SLCs on small cylinders, and they suggest that for experimental analysis of the SLC the β-number should be larger than 15 000 ($\beta = (2R)^2/\nu T$, with R the cylinder radius, T the local period of the wave, and ν the kinematic viscosity of the water). For the events presented in this paper, the longest wave corresponds to $\beta \approx 19\ 000$ and the Keulegan-Carpenter number is approximately 5, which places us in what they describe as cylinders of moderate size.

There has been a lot of work published around the relevance of the SLC for ringing responses. Grue and Huseby (2002) used the experimental data of the above-mentioned papers to show that SLCs and ringing responses are correlated, and state that "The secondary load cycle gives an important contribution to build-up of resonant body responses […]". High speed photography from the experiments of Chaplin et al. (1997) and Rainey and Chaplin (2003) was used by Rainey (2007) to conclude that "the rapid loading cycle causing the "ringing" vibration is traceable to local wave breaking around the cylinder […]". However, in a recent study, Paulsen et al. (2014) investigate the SLC numerically by solving the two-phase incompressible Navier-Stokes equations and conclude that "[…] the secondary load cycle is thus an indicator of strongly nonlinear flow rather than a direct contributor to the resonant forcing". This agrees with earlier findings from Krokstad and Solaas (2000), where a study of the phasing between the SLC and the ringing response led them to conclude that "The hydraulic jump [i.e. secondary load cycle] has no direct connection with the non-linear behaviour of the ringing force […]".

The paper is organized as follows: in section 2 we describe the experimental set up and the models used during the tests and section 3 gives a simple justification of how to estimate slamming events from video recording. Section 4 presents the analysis of the response of the flexible structure. Section 5 combines results from the stiff and the flexible structure to establish the link between secondary load cycle and ringing events. Conclusions of this study are drawn in section 6.

2. Presentation of the model test

The model tests were carried out at 1:30.6 scale, and Froude scaling was applied in order to correctly generate gravity waves. For the considered model and wave conditions, inertia forces dominate compared to viscous forces (DNV, 2014a; DNV, 2014b; IEC, 2009) and the effects of the Reynolds number mismatch are not examined here. All the values given in the paper are full-scale unless specified otherwise.

2.1. Test facilities

The tests were performed at the shallow water basin of MARIN, a 220 m long and 15.8 m wide wave flume (model scale) with constant water depth. One end of the flume was equipped with a piston-type wave-maker, consisting of a flat plate forced into horizontal translational motion by an electrical actuator. The wave maker includes 2nd order wave generation techniques that enable a correction for the difference between the oval motion of water particles in shallow/intermediate waters and the horizontal motion induced by the flat plate. It is possible to suppress parasitic wave generation using this technique (see Schäffer, 1996). On the other side of the flume, an absorbing parabolic beach was fitted in order to minimize wave reflection. Two pits were dug into the ground approximately 65 m (model scale) from the wave maker, and the two models were mounted onto two 6-component force frames solidly anchored into the pits. Figure 3 shows the layout of the experiment. No aerodynamic loading was modelled during the tests.

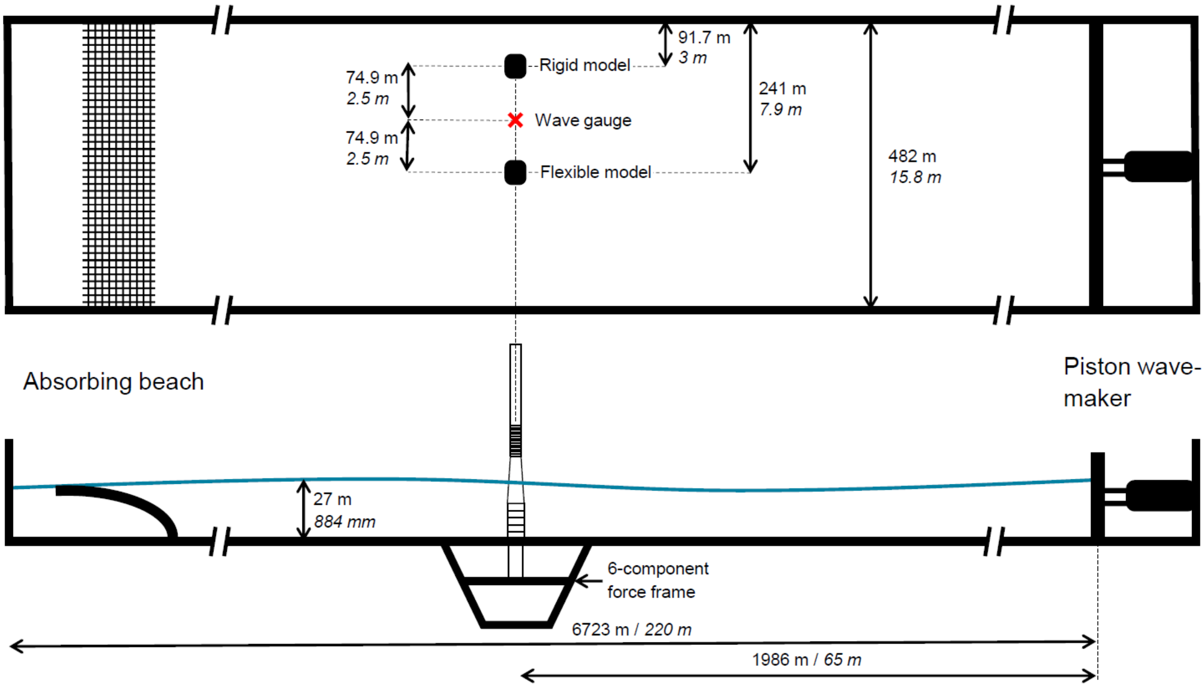

Figure 3. Top and side view of the experimental set-up (values are given both in full and model scale).

2.2. Physical models

2.2.1. Flexible model

A flexible model of an extra-large bottom-fixed offshore wind turbine mounted on a monopile was built according to typical dimensions of a 4 MW turbine. The model is composed of two cylindrical sections of diameters 7 m and 5.5 m, linked via a conical section (see Figure 4). This gives a diameter at the mean sea level of 5.8 m. The pile goes 10.1 m below seabed at a water depth of 27 m and extends up to 87 m above the mean sea level, for a total length of 124 m. The rotor-nacelle assembly is modelled by a mass of 278 tons placed at the top of the tower.

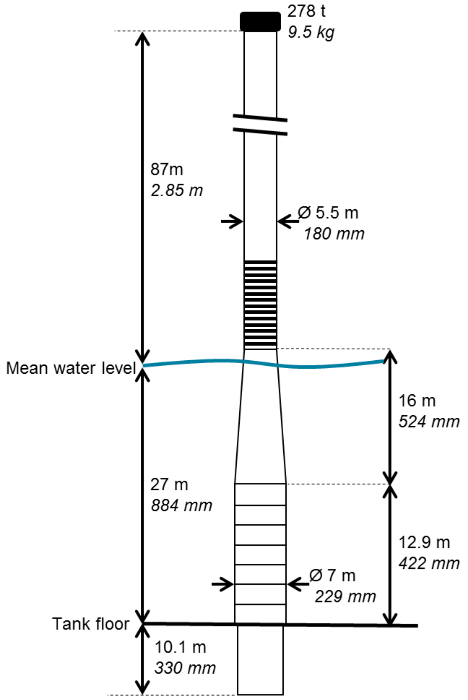

Figure 4. Characteristics of the flexible model (values are given both in full and model scale).

Special emphasis was put on achieving correct 1st and 2nd eigenfrequencies and the 1st mode shape. Table 1 gives the eigenfrequencies and damping values derived from hammer tests in water (Bunnik et al., 2015), and Figure 5 shows the targeted and obtained mode shapes of the flexible model. Due to physical restrictions in the laboratory, it is not straightforward to exactly match all mode shapes. The largest discrepancies occur at hub height which has little influence on the response to hydrodynamic loads. The obtained deflections at the mean sea level and down to the sea bed are seen to be acceptable.

The measured 3rd and 4th mode characteristics are also shown in Table 1 but they are not representative of the full-scale wind turbine. More details about the physical meaning of the 3rd and 4th mode are given in section 4.4.

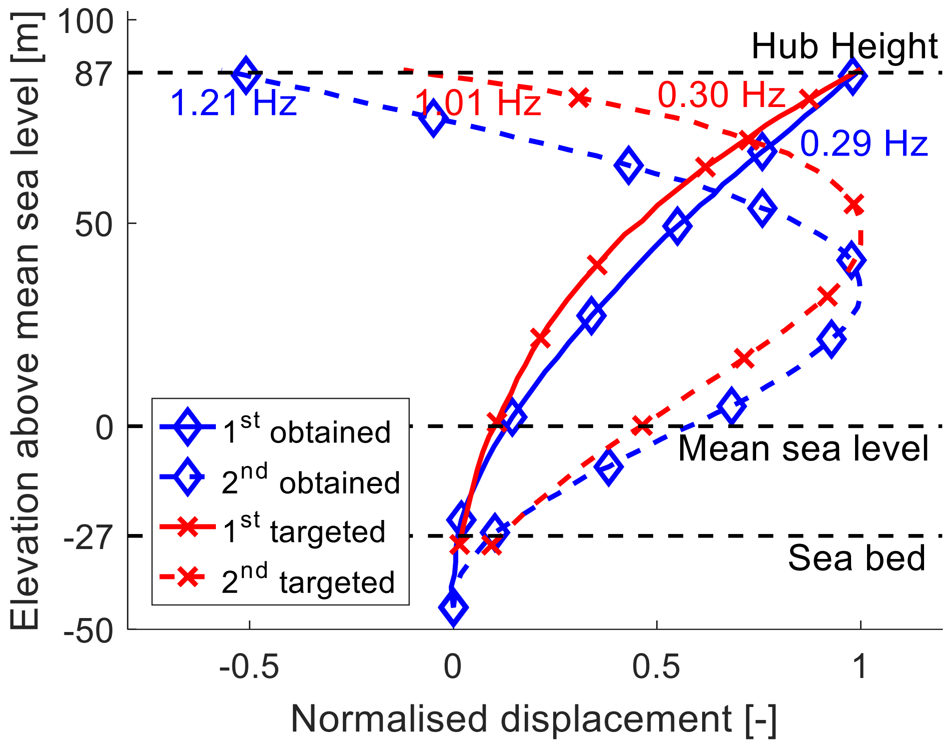

Figure 5. Dimensionless mode shapes. Blue colour represents the obtained mode shapes and red colour represents the targeted ones.

Table 1. Achieved frequencies and damping ratios of the flexible model (obtained from hammer tests).

	1st mode	2nd mode	3rd mode	4th mode
Eigenfrequency [Hz]	0.29	1.21	3.11	7.24
Damping (% of critical)	1.1	1.1	2	2

The damping for the first and second modes is found to be 1.1% of the critical damping. For the first mode, this is somewhat lower than the damping ratios measured on similar idling full-scale wind turbines (1.7 to 2.8% depending on the wind speed, Damgaard et al., 2013; Damgaard and Andersen, 2012; Shirzadeh et al., 2015). As a result, the obtained responses are expected to be slightly conservative, but previous research suggests that the damping is more important for the decay of the response than for the maximum values (Bachynski and Moan, 2014; Schløer et al., 2016).

2.2.2 Stiff model

A stiff model was also constructed, whose geometry is the same as the flexible model but extended only up to the expected maximum wave run-up. The objective of having a non-responding model was to be able to measure the hydrodynamic excitation.

Ideally, the 1st eigenfrequency of the stiff model should be as high as possible, such that it responds as little as possible to the hydrodynamic loading. The obtained fundamental eigenfrequency was 1.8 Hz (full-scale value). Figure 6 shows the smoothed spectrum of the measured wave elevation of one of the studied sea states (with a spectral peak period T_P = 10 s, see section 2.3). The wave spectrum does not contain significant energy at or above 0.4 Hz, i.e. one-third of the eigenfrequency of the stiff model, so 2nd and 3rd order excitation loads are not expected to excite significant response.

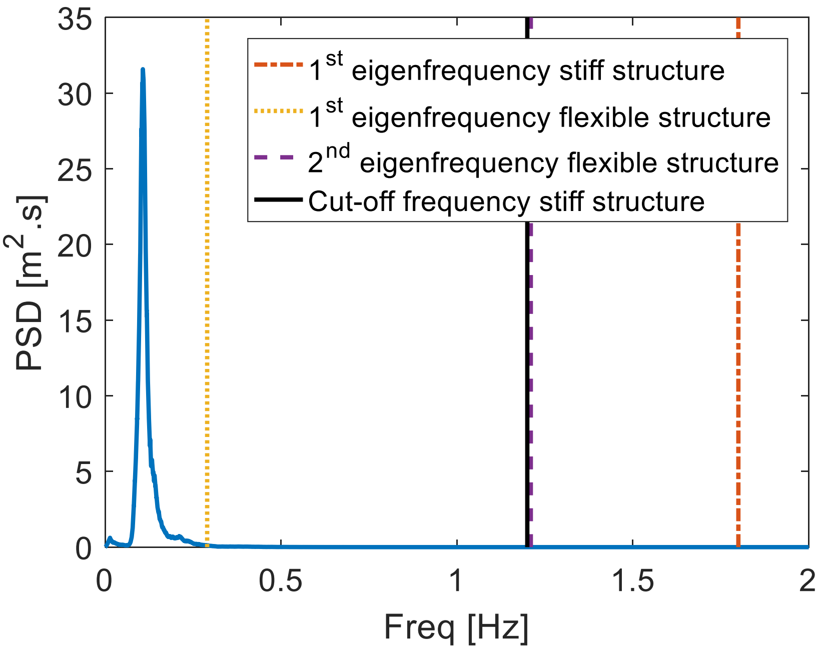

Figure 6. Example of an incoming wave spectrum.

During the tests, it was observed that the stiff model was nonetheless responding at times in its 1st mode. The loads measured on the stiff model can therefore not be taken as the excitation loads because they contain the dynamic amplification of the 1st mode of the structure. In order to remove the response from the stiff model from the measured response and keep only the excitation loads, a low-pass 6th order Butterworth filter was applied with a cut-off frequency at 1.2 Hz. This simple technique brings a major limitation: loads from breaking waves typically have very short durations, so by removing high frequencies from the excitation loads, the load contribution from breaking waves is potentially removed as well. The data from the stiff model therefore cannot be used to study slamming loads, but it can be used to examine 2nd and 3rd order loads.

2.2.3 Data acquisition

Foundation loads: Both models were placed on a 6 component measurement frame that enabled recording of forces and moments at the seabed.

Wave probes: 4 resistance-type wave probes were placed around the models to measure the wave elevation. One of the wave probes (marked with a red cross in Figure 3) was placed between the 2 models, at 2.4 m (model scale) from both of them (corresponding to around 13 diameters). It is expected that this wave probe is far enough from the models to not be affected by radiated and diffracted waves.

Video recording: Most sea states were recorded with two above-water cameras, one for each model. These video recordings are used to visually check whether a wave has broken when a large response of the structure was recorded (see section 3).

Accelerations: both models were fitted with accelerometers along their length. In the present study, those accelerometers were used to confirm that the flexible monopile only experienced significant displacement in the wave direction and to derive its mode shapes.

The wave elevations, loads and accelerations were recorded at a sampling rate of 200 Hz (model scale value), resulting in a time step of 5 ms in model scale, or 0.028 s in full scale.

2.3 Sea states

During the experiments, different irregular sea states were generated following a JONSWAP spectrum (Hasselmann et al., 1973). The JONSWAP spectrum describes sea conditions that are likely to occur for severe sea states in the North Sea and is typically recommended by the standards for ULS analysis (DNV, 2014a; DNV, 2014b; IEC, 2009). Table 2 shows the sea states that are analysed in this paper. For each sea state, only one realization was performed. Each sea state is characterized by a spectral peak period T_P and a significant wave height H_S. All sea states were realized with a spectral peak enhancement factor of 3.3.

We define an average wave steepness s_P for irregular seas based on (DNV, 2014b):

$$s_P = \frac{k_P H_s}{2\pi} \qquad (1)$$

where k_P is an average wave number obtained from T_P from the dispersion relationship (DNV, 2014b uses a linear dispersion relationship but we here apply eq (1) in Kirby and Dalrymple, 1986, which is based on 2nd order theory). For the analysed spectral peak periods, at the considered water depths, sea states with a steepness larger than 0.059 are not possible (DNV, 2014b). The average steepnesses used in this paper are well below this limit.

In addition, we calculate an averaged Ursell parameter Ur for the presented sea states. The Ursell parameter is typically defined for regular waves, but here we use the method given by Stansberg (2011) to calculate an average value for irregular seas:

$$Ur = \frac{k_p H_s}{2\left(k_p h\right)^3} \qquad (2)$$

where h is the water depth. The average Ursell numbers thus calculated are well below the classical limit of 0.33, above which 2nd order wave kinematic models are no longer valid and fully non-linear models are suggested.

Table 2. Selected sea states.

H_S	T_P	s_P	Ur
5.89	10	0.043	0.070
6.18	10	0.045	0.074
5.81	10.93	0.038	0.088

To give an indication of what these sea states represent in terms of return period, the H_S-T_P graph based on the metocean conditions at the Dogger Bank Creyke Beck B site is given in Figure 7 (see Frimann-Dahl, 2015). The yellow and blue lines correspond to 1-year and 5-year return period sea states, respectively, and the sea states are indicated with asterisks. More sea states than the ones analysed in this paper were run, but they are not presented here as they did not produce large responses of the structure.

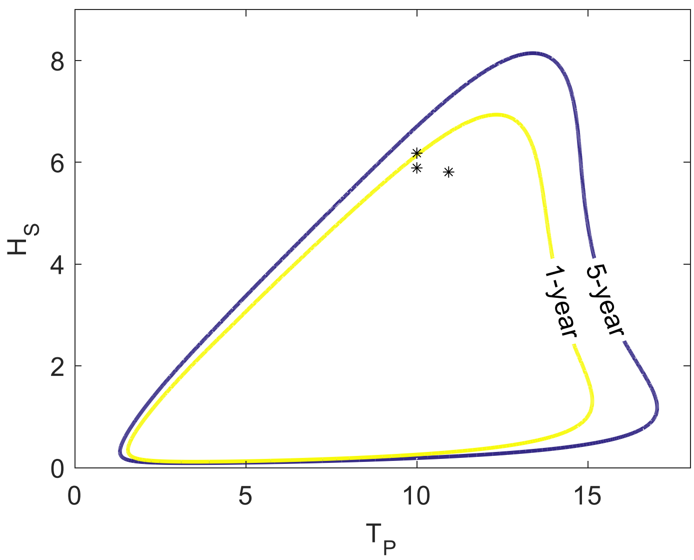

Figure 7. Contour lines for the metocean conditions at the Dogger Bank Creyke Beck B site. The asterisks represent the studied sea states.

When carrying out ULS analysis, the standards commonly used by the industry in the North Sea (DNV, 2014a; DNV, 2014b; IEC, 2009) recommend assessing sea states corresponding to 50-year return storms. The sea states considered in this paper correspond to generally much lower sea states, as illustrated by Figure 7, which is a limitation of this study. More extreme sea states were later tested with the same experimental set-up and will be included in future work.

It should also be noted that the wind conditions for the analysed sea states have not been determined. For the present paper and in the experiments, the turbine is assumed to be idling, which is likely not to be the case under the studied wave conditions. On an idling turbine, aerodynamic damping is usually small compared to an operating turbine (Shirzadeh et al., 2015) which makes 1st mode oscillations due to ringing decay slower than on an operating turbine (Bachynski and Moan, 2014; Schløer et al., 2016). This means that the ringing events observed during the experiments would decay faster if the turbine was operating.

3 Use of video recording to detect slamming on the flexible structure

Loads from breaking waves have been a major concern in the design of offshore structures over the past decades. We define 'slamming loads' for this paper using the explanation provided by Sarpkaya (1979): we consider a cylinder of radius R fixed to the sea bottom that we divide vertically into strips of length dz. We assume now that a vertical wall of incompressible water parallel to the cylinder with a control volume of constant mass per unit length M approaches a strip at a velocity u_0, the mass of water has then a horizontal momentum per unit length $p = Mu_0$. The duration of the impact being very short (Faltinsen, 1990; Sarpkaya, 2010) compared to the eigenperiod of the structure, it is reasonable to assume that, during the impact, no significant response will occur (according to classical structural theory, see for example Biggs, 1964) and that the cylinder will thus behave as a stiff structure. If we neglect nonconservative forces, the momentum of the water will remain constant during penetration. After the breaking wave has impacted the structure, because the fluid is in motion in the vicinity of the cylinder, a positive 2D added-mass term m_a appears, thus reducing the velocity to u and giving a new equation for the momentum $p = Mu_0 = (M + m_a)u$. Here m_a is taken as the high-frequency asymptote for the added mass (Faltinsen, 1990). Figure 8 illustrates the terms defined here, with the expression of the momentum p before and after impact. We can calculate the horizontal force using Newton's second law:

$$dF = \frac{dp}{dt}dz = \left((m_a + M)\frac{du}{dt} + u\frac{dm_a}{dt}\right)dz \qquad (3)$$

The first term of the above equation, proportional to the acceleration of the fluid, is the classical added mass load (see for example Faltinsen, 1990). The second term incorporating the time derivative of the added mass is the so-called slamming load dF_{slam}. If the latter is non-negligible compared to the former, the event is considered a slamming event.

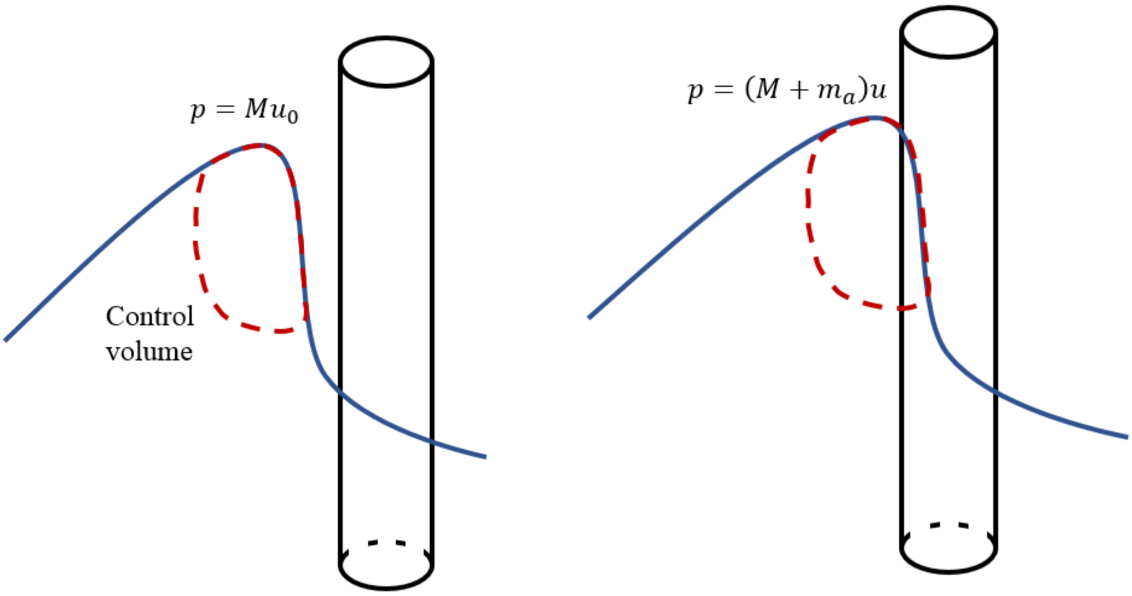

Figure 8. Breaking wave on circular cylinder before impact (left) and after impact (right).

This derivation provides a good mathematical understanding of slamming but is of little use in practice because the evaluation of the time-varying added mass is rather complex (Sarpkaya, 2010). However, it provides a way to visually check whether slamming loads occur. In order to have a large slamming force on a cylinder strip, we need to have a large velocity u in the horizontal direction and a rapidly changing two-dimensional added mass in the horizontal plane. For the considered monopile, the most suitable situation for slamming loads to occur is when a breaking wave impacts on the cylinder.

Under these conditions, most of the momentum of the water in motion will be in the horizontal direction. When the water particles impact the cylinder, they are restricted in the horizontal direction by the incoming water on the back side and by the cylinder itself on the front side. In order to conserve the total momentum, these particles must be deflected and ejected upwards and sideways, which gives a good visual indication of whether a slamming load has occurred. In the present paper, video recordings of the experiments are used to check whether slamming has occurred using the above hypothesis. Figure 10a,b show two such events.

4 Maximum response analysis

This section deals with the response of the flexible model and only data measured on this model is used here. Here and in the rest of the paper, the term ‘response’ corresponds to the bending moment of the flexible model taken at the seabed. A positive bending moment corresponds to the structure being deflected in the direction of the wave propagation. Since the amplitude of the moment is what is relevant to the design of a monopile rather than its direction, we compare absolute values of those moments. We therefore refer to ‘maximum’ or ‘highest’ moments even when the moment is negative.

In order to study the influence of different modes on the response of the structure, the measured bending moment in the frequency domain was split into responses around different frequencies corresponding to the eigenfrequencies of the system. Figure 9 below is the result of such decomposition performed on one of the events studied in this paper. The sum of the quasi-static, 1st and 2nd mode responses equal the total response. This figure enables us to assess the relative importance of the responses of different modes of the structure.

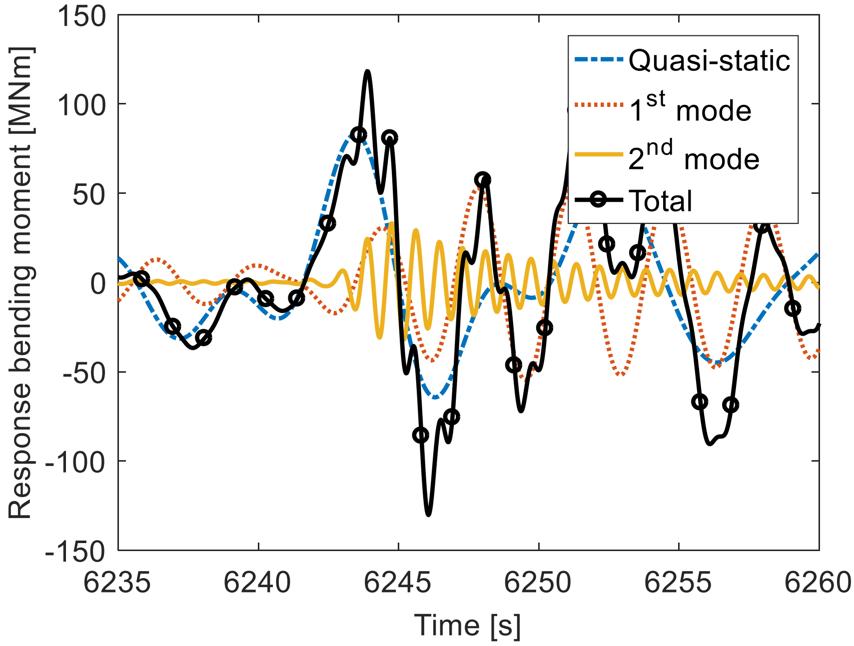

Figure 9. Example of decomposition of the response around the eigenfrequencies of the structure.

4.1 Maximum responses

In this section, the two events with the largest responses of all three sea states (named event 1 and event 2 and shown in Figure 10a,b respectively) are analysed in detail. Table 3 gives the characteristics of these two events. The trough-to-trough period is measured for each event and used to calculate the wave number k based on 2nd order theory (calculated with eq (1) in Kirby and Dalrymple, 1986), and η_m is the maximum wave elevation of the given event. The trough-to-trough period rather than the up- or down-crossing period was chosen because this type of wave is typically approximated by embedded stream function waves in design practices. The embedding process commonly uses the trough-to-trough period (Rainey and Camp, 2007).

Figure 10 shows these two events side to side. The figures from top to bottom correspond to the measured response and wave elevation, the frequency decomposition (as shown in Figure 9), the continuous wavelet transform (cwt) of the measured response, and snapshots of the cylinder at the time of wave impact. Responses from the 3rd and 4th modes of the structure have been removed by low-pass filtering, see section 4.4. Even though the contribution of these modes has been removed, we still refer to this filtered response as 'total response'.

Table 3. Events with maximum bending moments.

Event	Sea state	Max $[MNm]$	Time $[s]$	Period $[s]$	η_m $[m]$	k $[m^{-1}]$
1	$H_S = 5.89\ m, T_P = 10s$	-145	8848	7.80	6.61	0.0599
2	$H_S = 6.18\ m, T_P = 10\ s$	-130	6246	8.13	7.57	0.0550

For these events, the maximum response is measured when a steep and breaking wave passes the structure (see Figure 10c,d). The wave excites the 1st mode of the structure, which starts oscillating and decays in similar fashion to the ringing phenomenon described in section 1. As shown in Figure 10e,f , the structure also oscillates in its 2nd mode, but in a different way than the 1st mode response: the 2nd mode resonant oscillations occur suddenly after the breaking wave has passed, whereas the 1st mode response experiences a build-up over one wave period and then slowly decays. The influence of the second mode is studied in more detail in the following section.

The cwt plots of Figure 10g,h also show that the structure responds at the frequency of the wave (about 0.1 Hz for the selected events) and that its 1st and 2nd modes are triggered (respectively at 0.29 and 1.21 Hz). The snapshots of Figure 10a,b indicate that the wave breaks at the cylinder. As explained in the previous section, the water particle ejection visible in the photographs is characteristic of slamming events.

Event 1

a. Snapshot of event 1

Event 2

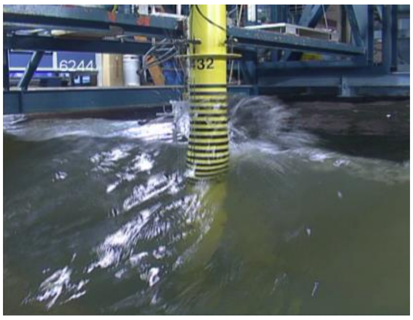

b. Snapshot of event 2

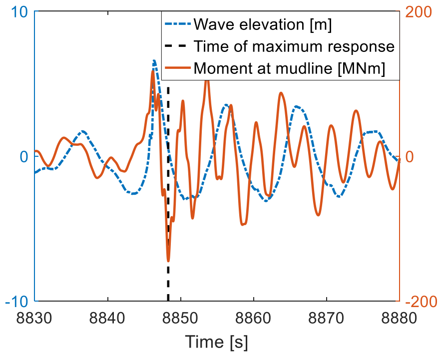

c. Response and wave elevation of event 1

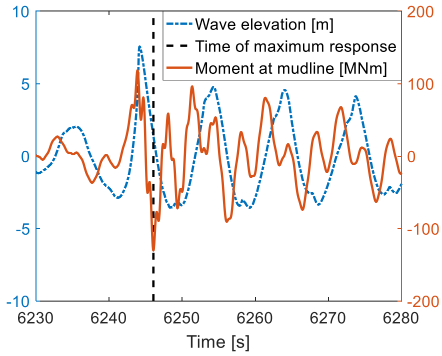

d. Response and wave elevation of event 2

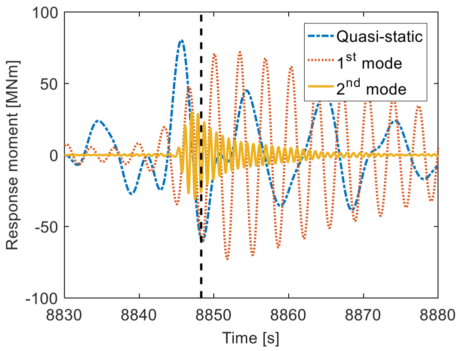

e. Response decomposition of event 1

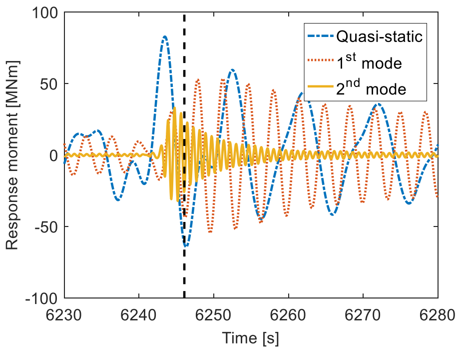

f. Response decomposition of event 2

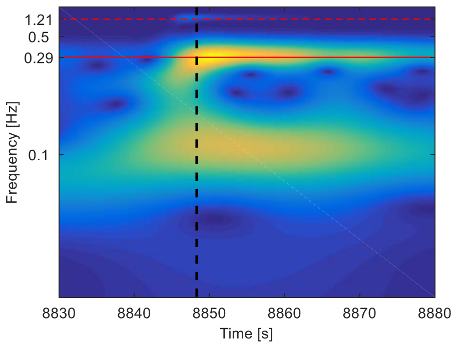

g. Cwt of event 1

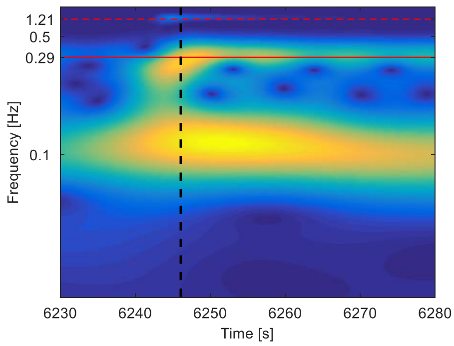

h. Cwt of event 2

Figure 10. Characteristics of the largest and 2nd largest measured responses, respectively Event 1 and 2.

In addition to the two events shown in Figure 10, the 21 events with the largest responses were analysed. For all events it was found that the 1st and 2nd mode responses were triggered after the passage of a steep and breaking wave, as described above. The characteristics of these 21 events are given in Table 5.

Previous work done by Suja-Thauvin et al. (2016) and further developed by Suja-Thauvin and Krokstad (2016), showed that the first mode response of a similar structure can be explained solely by 2nd and 3rd order hydrodynamic excitation loads, without the need to account for slamming loads. We apply their findings to the present study to conclude that the ringing response observed for large events is mainly due to 2nd and 3rd order hydrodynamic loads and not to slamming loads. However, as their work is done on a one degree-of-freedom system, it does not include any consideration of the 2nd mode of the structure.

4.2 Contributions to the total response

In this section, we analyze the contribution of the different modes of the structure to the total response. To do so, we decompose the response as shown in Figure 9 and Figure 10c,d and evaluate the value of the response at different modes at the instant of maximum total response. Their relative importance for events 1 and 2 is given in Table 4. Moments (here and in the rest of the paper) are given within an accuracy of 3%.

Table 4. Different contributions to the maximum load.

Event	Total moment [MNm]	% quasi-static	% 1st mode	% 2nd mode
1	-145	41.1	41.6	17.2
2	-130	48.3	33.2	18.5

Figure 11 offers a graphical interpretation of table 4 for the 21 largest events. This figure shows the different contributions to the total response: quasi-static response accounts for between 40 and 60%, 1st mode response accounts for between 30 and 40% and the second mode contributes up to 20%. The numerical values for each event are given in Table 5.

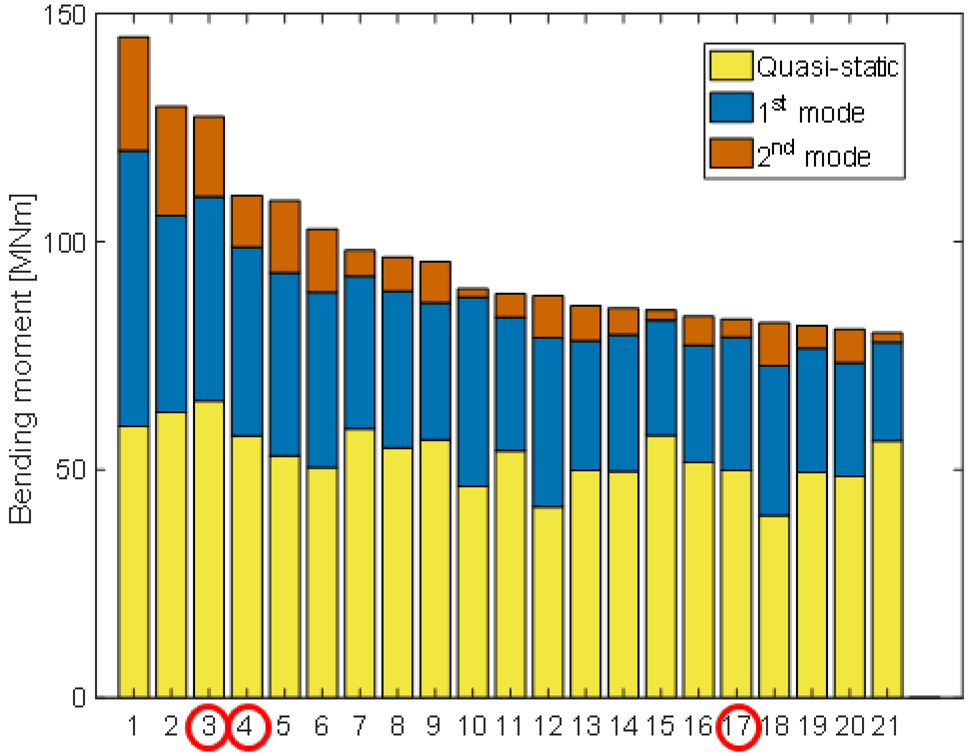

Figure 11. Decomposition of the largest responses into quasi-static, 1st and 2nd mode response. The red circles correspond to events where no secondary load cycle was observed (see section 5).

These observations suggest, as was also found in de Ridder et al. (2011), that not taking into account the 2nd mode of the structure when assessing ULS leads to underestimation of the total response. For these 21 events, we also note that the maximum response is negative, i.e. it corresponds to the structure moving against the wave propagation direction.

Table 5. Characteristics of the 21 highest recorded responses. T, η_m, H and k correspond to the trough-to-trough wave period, the crest elevation, the wave height and the wave number, respectively.

Event	Max $[MNm]$	Contribution to total moment [%]			Time $[s]$	Sea state Hs - Tp	T [s]	η_m $[m]$	H $[m]$	k $[m^{-1}]$
		Quasi-static	1st mode	2nd mode						
1	-145	41.1	41.6	17.2	8848	5.89 m – 10 s	7.82	6.61	9.32	0.0599
2	-130	48.3	33.2	18.5	6246	6.18 m – 10 s	8.15	7.57	10.6	0.055
3	-127	51.1	35.1	13.7	1046	5.89 m – 10 s	8.76	8.06	11.96	0.0492
4	-111	52.2	37.6	10.2	3132	6.18 m – 10 s	7.24	6.65	9.02	0.0664
5	-110	48.8	36.7	14.5	6962	6.18 m – 10 s	9.34	6.33	9.67	0.0474
6	-103	49.2	37.3	13.5	10688	5.89 m – 10 s	7.57	5.85	8.45	0.0642
7	-98.2	60.2	34.0	5.8	340	6.18 m – 10 s	8.62	6.43	9.53	0.0527
8	-97.0	56.8	35.5	7.7	6961	5.89 m – 10 s	9.29	7.4	10.23	0.0465
9	-95.7	59.2	31.4	9.4	4217	5.81 m – 10.93 s	7.96	6.52	8.57	0.0587
10	-88.6	51.8	46.1	2.1	6482	5.89 m – 10 s	8.82	6.12	9.51	0.0516
11	-88.6	61.3	32.9	5.8	8748	5.89 m – 10 s	7.63	5.67	8.3	0.064
12	-86.3	47.5	42.1	10.4	4514	5.81 m – 10.93 s	10.59	6	8.64	0.0405
13	-86.0	58.2	33.0	8.9	6685	6.18 m – 10 s	7.96	5.83	8.01	0.0599
14	-85.7	58.2	34.9	6.9	5293	6.18 m – 10 s	8.71	7.08	10.06	0.0511
15	-85.1	67.8	29.6	2.6	6245	5.89 m – 10 s	8.71	6.57	10.09	0.0518
16	-83.6	61.8	30.6	7.6	6562	5.89 m – 10 s	8.46	5.79	8.53	0.0551
17	-83.2	60.2	35.1	4.8	8583	5.89 m – 10 s	7.43	7	9.54	0.0633
18	-82.5	48.7	39.9	11.4	8616	5.81 m – 10.93 s	10.14	5.69	7.74	0.0431
19	-81.6	60.6	33.3	6.1	2304	6.18 m – 10 s	7.13	4.67	6.5	0.073
20	-80.9	60.2	30.8	9.0	9499	5.89 m – 10 s	8.12	6.09	8.82	0.0578
21	-80.1	70.5	267.0	2.5	11492	5.81 m – 10.93 s	10.06	7.18	10.41	0.0421

It should be noted that Table 5 only shows the characteristics of the individual waves that occur at the same time as the maximum response. However, a wave with a given height could produce less response than a wave with smaller height if, for the latter case, the structure was already responding to a previous wave. This "memory effect" is relevant for dynamic systems with low damping. Peng et al. (2013) showed that wave groups could produce larger responses than individual regular waves with the same characteristics as the largest wave of the wave group.

4.3 Physics of the second mode response

Figure 12 shows the full time series of the 2nd mode response of sea state H_S = 6.18 m and T_P = 10 s. In this plot, independent peak occurrences of 2nd mode response higher than half of the standard deviation of the quasi-static response have been marked with a red dot. From comparison with the video recordings, it appears that these large second mode responses only occur when a breaking wave hits the cylinder. Indeed, as pointed out by Hallowell et al. (2015), loads from breaking waves have two characteristics that make them especially relevant when analysing 2nd mode motion:

- They have a very short duration (as shown for instance by Wienke and Oumeraci, 2005) compared to 1st, 2nd or 3rd order loads (Suja-Thauvin and Krokstad, 2016). With such a duration, according to classical structure theory (see for example Biggs, 1964), these loads have the potential to trigger significant 2nd mode response.
- They are concentrated around the free water surface, where 2nd mode shape displacement is the highest (see Figure 5) whereas loads from non-breaking waves are distributed between the free surface and the sea bed.

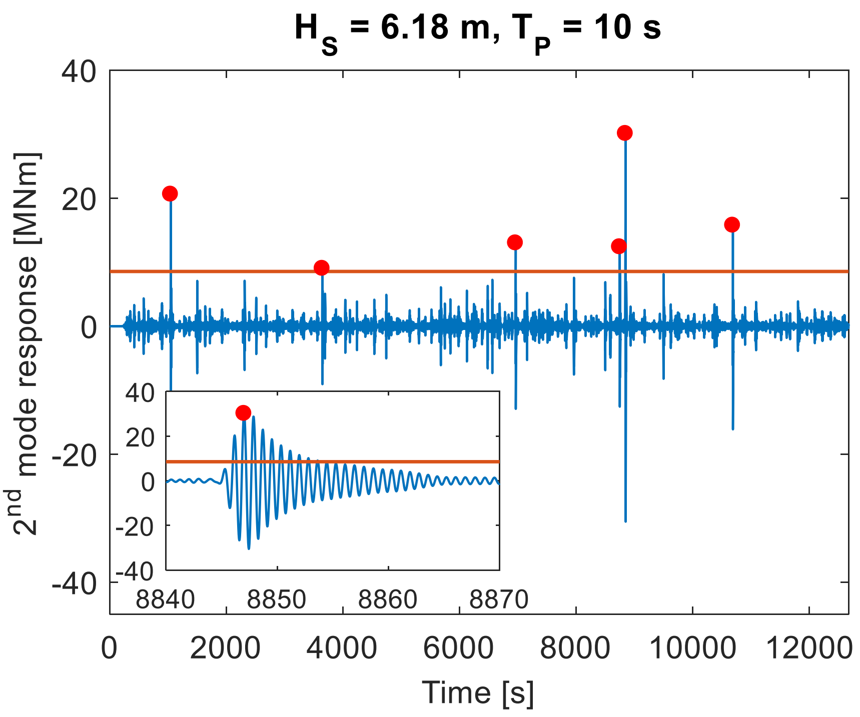

Figure 12. Response of the structure in its 2nd mode. A zoom of the 2nd mode response of event 1 is also shown. The red line corresponds to half of the standard deviation of the quasi-static response.

This visual check was performed for all sea states mentioned in this paper, and it was consistently found that responses of the 2^{nd} mode above the selected threshold corresponded to breaking wave events. We therefore suggest that large 2^{nd} mode responses only occur when a wave breaks at the cylinder. However, it should be noted that not all breaking wave events produce such a large response in the 2^{nd} mode.

The empirical cumulative distribution function of the 2nd mode response is given in Figure 13 in terms of exceedance probability. Exceedance probabilities for total and the quasi-static response are also shown for comparison. There is a qualitative difference between the 2^{nd} mode response and the other responses: for the main part of the observations (for an exceedance probability higher than about 3% for the most severe sea states or even than 0.5% for the mildest sea state), the probability of exceedance curve of the 2^{nd} mode response follows a linear variation (in the logarithmic plot). For lower exceedance probabilities, the 2^{nd} mode response significantly increases. This sudden change in the slope of the probability of exceedance curve is not visible for the total or the quasi-static response.

In order to explain this observation we compare the 2^{nd} mode response to the quasi-static response. A given wave produces a quasi-static response proportional to the wave particle acceleration for an inertia-dominated structure such as the one presented here. The quasi-static response is therefore roughly linear in terms of wave steepness. The 2^{nd} mode, however, is only triggered by breaking waves, which means that below a certain steepness threshold, no 2^{nd} mode response is expected, but past this threshold the 2^{nd} mode gets excited and large responses will occur. This confirms the non-linear behaviour of 2^{nd} mode response and shows that there will be a large number of outliers in the peak distribution.

In addition, the excess kurtosis gives a good indicator of the behaviour of the outliers of a given distribution. The excess kurtosis (calculated for each sea state using all data points) is calculated by Matlab® with the following formula:

$$k_1 = \frac{\frac{1}{n}\sum_{i=1}^{n}(x_i - \bar{x})^4}{\left(\frac{1}{n}\sum_{i=1}^{n}(x_i - \bar{x})^2\right)^2} - 3 \qquad (4)$$

where n is the number of samples, x is the set of data points and $\bar{x}$ is the average of x. A large excess kurtosis means that the distribution produces a large number of outliers and that their value will be more extreme than for a normal distribution. For the presented sea states, the 2^{nd} mode response has a very large excess kurtosis compared to the total and quasi-static responses, as shown in Table 6. This confirms what was suggested in the previous paragraph, i.e. that the extremes of the 2^{nd} mode response lie far from the rest of observations.

Table 6. Excess kurtosis of the measured wave (W_{meas}), of the total (M_{tot}), quasi-static (M_0) 1st mode (M_1) and 2nd mode (M_2) moments.

	W_{meas}	M_{tot}	M_0	M_1	M_2
$H_S = 6.18\ m,\ T_P = 10\ s$	-0.0543	0.787	0.0667	3.83	190
$H_S = 5.89\ m,\ T_P = 10\ s$	0.0538	0.915	0.185	4.91	147
$H_S = 5.81\ m,\ T_P = 10.93\ s$	0.0020	0.370	0.0704	1.10	33.3

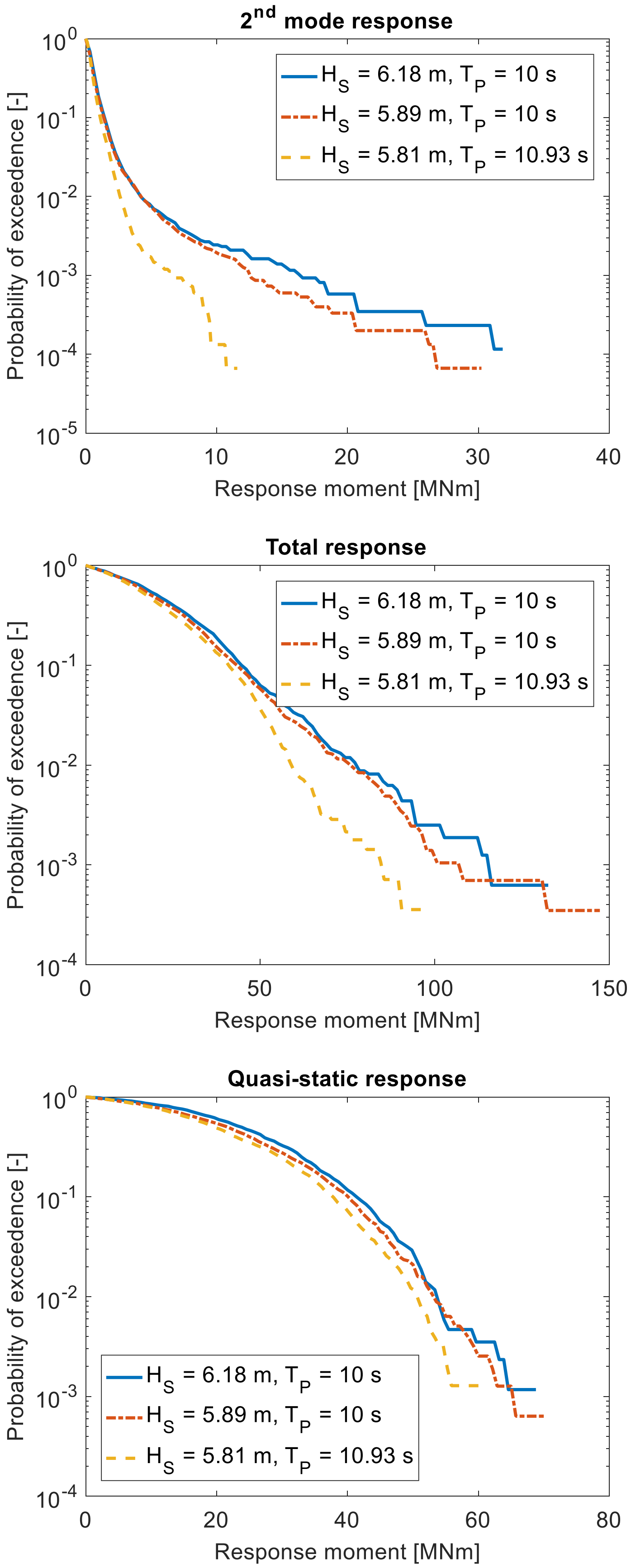

395 **Figure 13. Empirical exceedance probability curve for response moments.**

4.4 3rd and 4th modes

The previous analysis considered measured responses after filtering out the 3rd and 4th mode. However, these modes are in fact present and they contribute to the total measured response. As exemplified in Figure 14 (a zoom of event 2), structural modes higher than the 2nd mode influence the response. These modes decay quickly after the slamming impact.

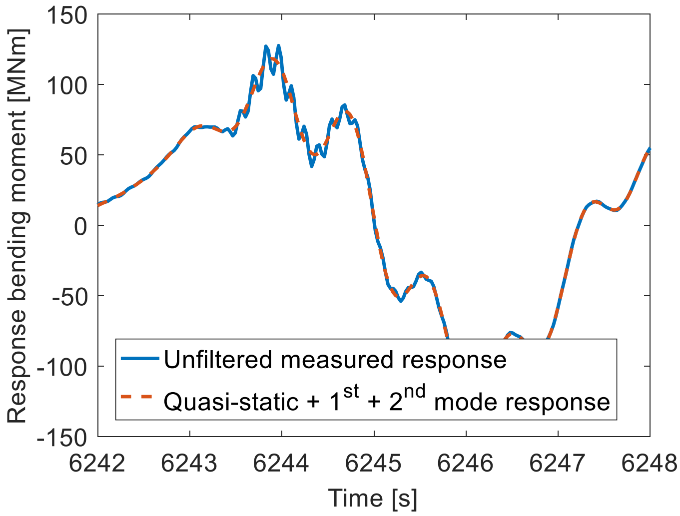

Figure 14. Zoom of the response of event 2. The difference between the two curves is due to modes higher than 2nd.

Figure 15 shows a zoom of the wavelet plot for event 2 (the scaling of the colours has been changed compared to Figure 10 for clarity). This plot shows that the 3rd and 4th modes, respectively at 3.11 and 7.24 Hz are also excited by the breaking wave but that their influence is limited compared to the 2nd mode response at 1.21 Hz.

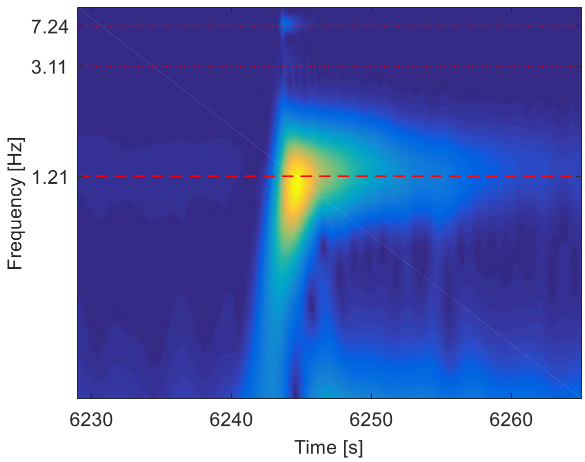

Figure 15. Zoom of the cwt plot of the unfiltered measured response of event 2.

The 3rd and 4th modes on the model were not tuned to fit the modes of a full-scale wind turbine, so the response at these modes is not representative of that of a full-scale wind turbine. Further analysis of the influence of higher modes is needed to assess their influence on the total response of an offshore wind turbine, and whether not including 3rd and 4th modes might lead to non-conservative results.

5 Secondary load cycle analysis

In this section we use data measured on the stiff model and on the flexible model. Both models were in the basin at the same time and experienced the same sea states.

5.1 Occurrences in the present study

The secondary load cycle (SLC) appears as a rapid and high-frequency variation in the excitation force. Figure 16 shows an occurrence of a SLC together with the definitions of its magnitude (F_{SLC}) and the peak-to-peak force (F_{PP}). The SLC ratio is defined as F_{SLC}/F_{PP} (Grue and Huseby, 2002).

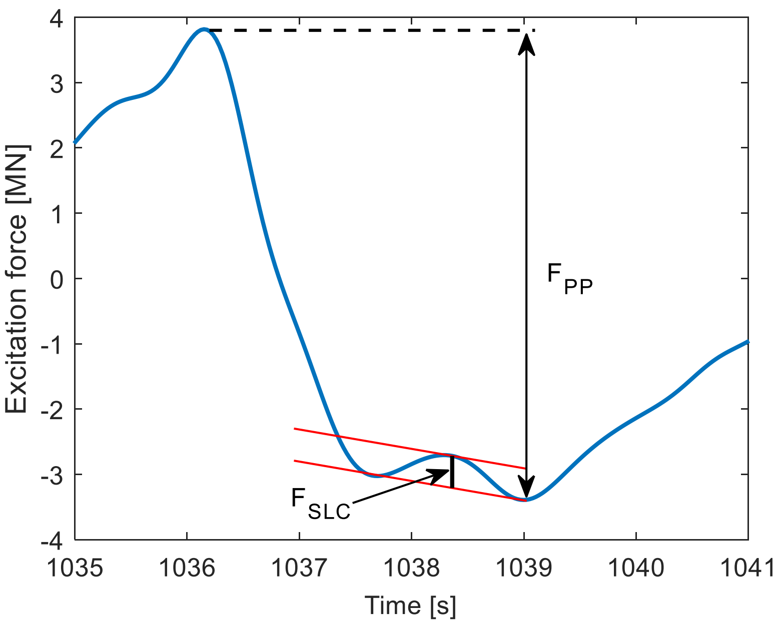

Figure 16. Example of a secondary load cycle occurrence with the definitions of the magnitude and the peak-to-peak force.

The occurrences of SLCs are found by analysing the force measured by the stiff structure. As explained in section 2.2.2, this measured force is first low-pass filtered at a frequency of 1.2 Hz to remove the response of the structure, giving the time-series obtained in Figure 16. Grue et al. (1993) state that the SLC has a duration of about 15% of the wave period. For the present experiments, this corresponds to durations of about 1.5 s. The cut-off frequency is about twice the expected frequency of the SLC; it is therefore expected that the SLC is not removed or significantly altered by the filtering. A visual check of the excitation force time series is performed on each of the events selected hereafter to ensure they correspond to SLCs.

For each of the three sea states, the 25 occurrences of SLCs with the highest magnitudes are kept and plotted in the $kR - k\eta_m$ plane in Figure 17. Our observations of SLCs are within the same range as those reported by Grue and Huseby, (2002) where they report SLCs for $0.1 < kR < 0.21$ and $0.2 < k\eta_m < 0.33$. They analysed the SLC phenomenon based on experiments carried out in deep water, whereas the experiments of the present paper were performed in finite water. It should be noted that due to finite water, we observe SLC for waves steeper than those reported in Grue and Huseby (2002). This is the only noticeable difference between SLC occurrences in deep water and finite water.

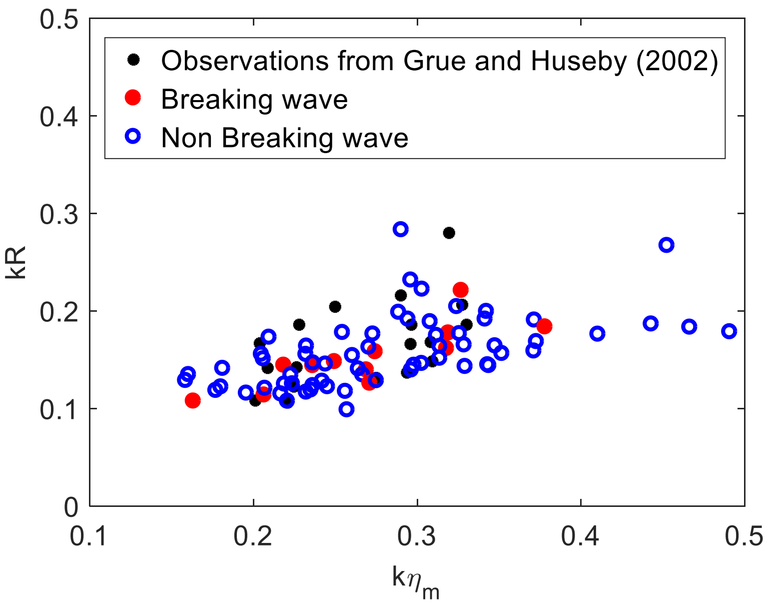

Figure 17. Occurrences of secondary load cycle in the kR - $k\eta_m$ plane. The 25 largest occurrences (i.e. with highest magnitudes) of each of the 3 sea states are kept.

5.2 Link with maximum responses

The correlation between SLC and ringing responses was examined in the present experiments. For each of the 75 occurrences, the response of the structure in its 1st mode is analysed: the maximum of the 1st mode response (measured on the flexible structure) occurring immediately after the SLC is normalized by dividing it by the excitation moment (measured on the stiff structure). The obtained result is plotted as a function of the SLC ratio in Figure 18.

Figure 18 shows that the highest 1st mode amplifications are not provoked by the largest SLC ratios. Breaking waves usually provoke large 1st mode amplification, but as explained previously, there is no causality link between the two phenomena: both are a consequence of a wave being very steep.

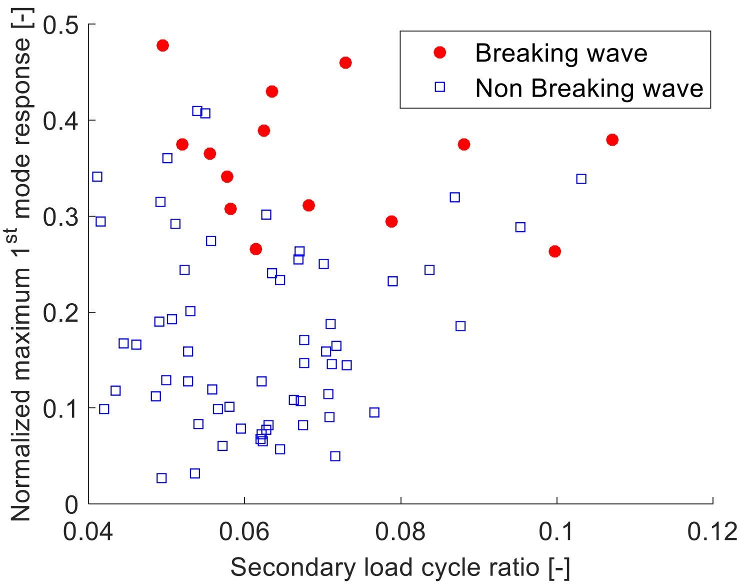

Figure 18. Correlation between the secondary load cycle ratio and the 1st mode amplification. The 25 largest occurrences (i.e. with highest magnitudes) of each of the 3 sea states are kept.

Another correlation that was explored is the time of occurrence of the SLC against the 1st mode response amplification. The time of occurrence is defined as the time between the maximum of the excitation force and the maximum of the SLC, and is normalized by the wave period. Again, there is no clear trend between the time of occurrence and the 1st mode amplification.

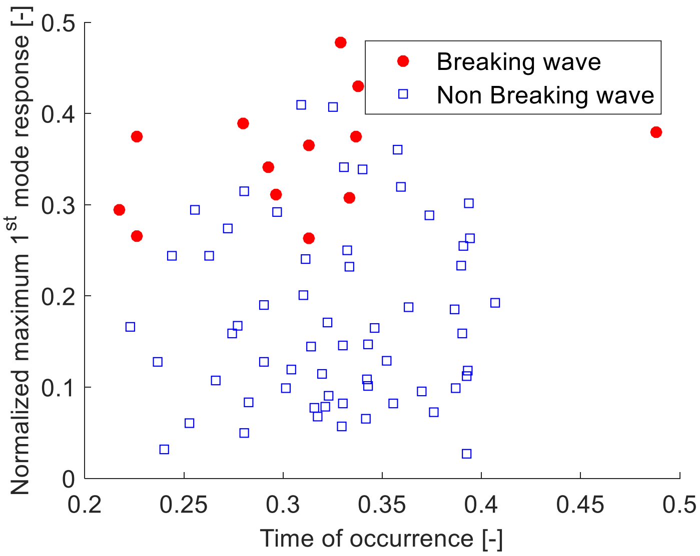

Figure 19. Correlation between the time of occurrence of the secondary load cycle and the 1st mode amplification. The 25 largest occurrences (i.e. with highest magnitudes) of each of the 3 sea states are kept.

In addition, some events did not present a SLC but a ringing type of response was still visible in the bending moment (these events are marked with a red circle in Figure 11). Figure 20 shows events 3 and 4 (respectively 3rd and 4th highest total responses) in detail. No SLC was seen in the measured excitation for either event. However, the lower plots of Figure 20 clearly show a resonant response of the structure around its first eigenfrequency, characteristic of ringing responses.

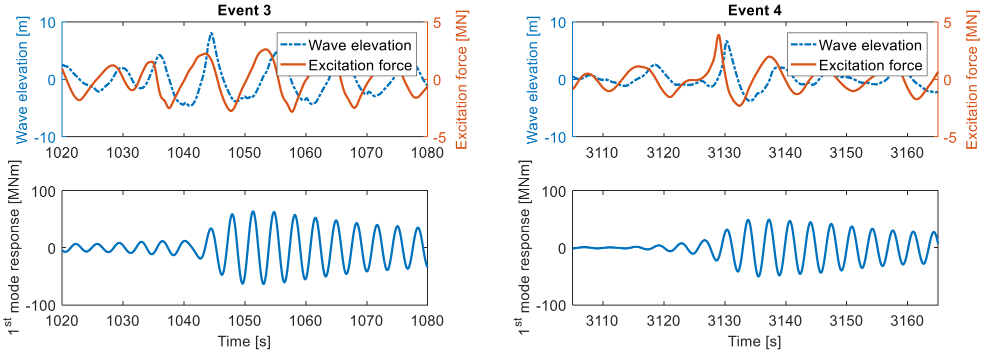

Figure 20. Large response events with no visible secondary load cycle. The response is measured on the flexible model while the excitation is measured on the stiff one.

These observations suggest that in the present experiment, the SLC is not a necessary load attribute to generate ringing response. This statement has important implications in terms of what is necessary to accurately model the response of offshore wind turbines in ULS conditions. Faltinsen et al. (1995) and Malenica and Molin (1995) developed third-order hydrodynamic models based on a perturbation approach (with the wave steepness as the perturbation parameter) in order to model ringing events. These models, as was shown in Paulsen et al. (2014), cannot depict the SLC because it is a phenomenon of even higher order.

However, as discussed in this paragraph, the SLC is not required in the excitation force to produce ringing responses, meaning that these models that cannot predict SLCs can still potentially predict ringing responses, as seen for deep water (Gaidai and Krokstad, 2014).

6 Conclusions

Experimental data of a bottom-fixed offshore wind turbine mounted on a monopile and subjected to extreme weather conditions in finite water are analysed in this paper. Two models of the support structure are presented: one is a fully flexible model whose 1st and 2nd eigenfrequencies and 1st mode shape were tuned to fit those of a full scale 4 MW wind turbine and the other one is a stiff model with the same dimensions as the flexible model. Both models were in the tank at the same time and therefore experienced the same incoming waves.

The flexible model is used to study the bending moment response at the seabed of the structure in ULS conditions. Over the whole set of experiments, the 21 events with largest responses are analysed and the bending moment is decomposed into response around the 2nd eigenfrequency, response around the 1st eigenfrequency (which highlights ringing responses) and quasi-static response. It is found that for every event, in addition to the quasi-static response, the structure experiences ringing and that its second mode is triggered, contributing to up to 20% of the total response. In line with what was found in Suja-Thauvin and Krokstad (2016) and by comparing the bending moment time series with video recordings, the conjecture is made that ringing responses are induced by 2nd and 3rd order hydrodynamic loads and that the 2nd mode is excited by slamming loads. The 2nd mode response exhibits behaviour qualitatively different than the total response or the quasi-static response. By analysing the excess kurtoses of the 2nd mode response of different sea states and the exceedance probability, it is shown that there are more outliers with more extreme values in the 2nd mode response than in the total or quasi-static response.

The excitation force is obtained by measuring the force at the stiff structure. This enables study of the phenomenon known as secondary load cycle, where shortly after the passage of a steep wave, a high frequency increase of the excitation force occurs. It has been conjectured in previous work that the secondary load cycle could be a cause of ringing responses. In the present paper, however, no correlation is found between the characteristics of secondary load cycles and ringing responses. Furthermore, some events with a strong ringing response do not present a secondary load cycle in the excitation force, indicating that the secondary load cycle is not a necessary load attribute to trigger ringing responses.

There are several important limitations to the present work, which is based on a limited number of experimental realizations at 1:30 scale. In addition to the limitations and uncertainties associated with small-scale testing and wave generation, this study only deals with one pair of values for 1st and 2nd eigenfrequencies. With the current trend of rotors getting larger (Ho et al., 2016), it is expected that the mass and moment of inertia on top of the tower will increase differently, thus changing the ratio of 1st over 2nd eigenfrequency. This could potentially change the relative contributions of the 1st and 2nd mode responses to the total response and therefore modify Figure 11. A more detailed assessment of this phenomenon is left for further studies. The presence of the 3rd and 4th mode in the response, and the use of visual detection of slamming also represent limitations in the present work. Furthermore, the sea states considered here are not associated with a 50-year return period. As such, the considered conditions are not necessarily representative of typical ULS assessment, and the assumption of an idling turbine may not be correct. Finally, memory effects (i.e. the fact that the response to one wave depends on the response to previous waves) are not studied in this paper. As explained in section 4.2, wave groups can produce larger responses than individual regular waves with the same characteristics as the largest wave of the wave group.

This study explains the mechanism of large responses in ULS conditions for offshore wind turbines and shows the necessity of having both a non-linear hydrodynamic load model and a slamming model for the excitation loads, and at least 1st and 2nd structural modes accurately represented. The finite water conditions make it likely that more and steeper breaking waves will occur at the support structure of the turbine compared to deep water. In order to account for the phenomena described in this paper, a common practice in the industry is to simulate the wave kinematics using the stream function theory (Rienecker and Fenton, 1981) and adding a slamming model on top of it. This model will be studied in depth in future work.

Acknowledgments

This study has been financed by Statkraft and the Norwegian Research Council, project number 237192. The authors are grateful to the WiFi project for providing the experimental data used for this paper as well as for support and relevant input to the presented discussion. The participants of the WiFi project, in alphabetical order, are Ballast Nedam, Deltares, DNV, Dong, ECN, EON, GL, MARIN, Ramboll, Royal HaskoningDHV, RWE, Savannah River National Laboratory, Siemens, Sirris/OWI-lab, Statkraft, Statoil, STX, Van Oord, Vattenfall and Volker InfraDesign bv.

References

Bachynski, E.E., Moan, T., 2014. Ringing loads on tension leg platform wind turbines. Ocean Eng. 84, 237–248. doi:10.1016/j.oceaneng.2014.04.007

Biggs, J.M., 1964. Introduction to structural dynamics. McGraw-Hill College.

Bredmose, H., Slabiak, P., Sahlberg-Nielsen, L., Schlütter, F., 2013. Dynamic Excitation of Monopiles by Steep and Breaking Waves: Experimental and Numerical Study V008T09A062. doi:10.1115/OMAE2013-10948

Bunnik, T., Helder, J., de Ridder, E.J., 2015. Simulation of the Flexible Response of a Fixed Offshore Wind Turbine subject to Breaking Waves. Presented at the 7th International Conference on HYDROELASTICITY IN MARINE TECHNOLOGY.

Chaplin, J.R., Rainey, R.C.T., Yemm, R.W., 1997. Ringing of a vertical cylinder in waves. J. Fluid Mech. 350, 119–147. doi:10.1017/S002211209700699X

Dalrymple, R.A., Dean, R.G., 1991. Water wave mechanics for engineers and scientists. Prentice-Hall.

Damgaard, M., Andersen, J.K.F., 2012. Natural Frequency And Damping Estimation of an Offshore Wind Turbine Structure. Presented at the The Twenty-second International Offshore and Polar Engineering Conference, International Society of Offshore and Polar Engineers.

Damgaard, M., Ibsen, L.B., Andersen, L.V., Andersen, J.K.F., 2013. Cross-wind modal properties of offshore wind turbines identified by full scale testing. J. Wind Eng. Ind. Aerodyn. 116, 94–108. doi:10.1016/j.jweia.2013.03.003

de Ridder, E.J., Aalberts, P., van den Berg, J., Buchner, B., Peeringa, J., 2011. The Dynamic Response of an Offshore Wind Turbine With Realistic Flexibility to Breaking Wave Impact 543–552. doi:10.1115/OMAE2011-49563

DNV, 2014a. DNV-OS-J101 Design of offshore wind turbine structures. DNV.

DNV, 2014b. DNV-RP-C205 Environmental Conditions and Environmental Loads. DNV.

Faltinsen, O.M., 1990. Sea loads on ships and offshore structures, Ocean Techmology. Cambridge.

Faltinsen, O.M., Newman, J.N., Vinje, T., 1995. Nonlinear wave loads on a slender vertical cylinder. J. Fluid Mech. 289, 179–198. doi:10.1017/S0022112095001297

Frimann-Dahl, J., 2015. Experimental Validation and Design Review of Wave Loads on Large-Diameter Monopiles. NTNU, Marine Technology.

Gaidai, O., Krokstad, J., 2014. Extreme Response Statistics of Fixed Offshore Structures Subjected to Ringing Loads. J. Offshore Mech. Arct. Eng. 136, 031604–031604. doi:10.1115/1.4027542

Grue, J., Bjørshol, G., Strand, Ø., 1993. Higher harmonic wave exciting forces on a vertical cylinder.

Grue, J., Huseby, M., 2002. Higher-harmonic wave forces and ringing of vertical cylinders. Appl. Ocean Res. 24, 203–214. doi:10.1016/S0141-1187(02)00048-2

Hallowell, S., Myers, A.T., Arwade, S.R., 2015. Variability of breaking wave characteristics and impact loads on offshore wind turbines supported by monopiles. Wind Energy n/a-n/a. doi:10.1002/we.1833

Hasselmann, K., Barnett, T.P., Bouws, E., Carlson, H., Cartwright, D.E., Enke, K., Ewing, J.A., Gienapp, H., Hasselmann, D.E., Kruseman, P., Meerburg, A., Müller, P., Olbers, D.J., Richter, K., Sell, W., Walden, H., 1973. Measurements of wind-wave growth and swell decay during the Joint North Sea Wave Project (JONSWAP).

Ho, A., Mbistrova, A., Corbetta, G., 2016. The European offshore wind industry - key trends and statistics 2015 [WWW Document]. WindEurope. URL https://windeurope.org/about-wind/statistics/offshore/key-trends-2015/ (accessed 10.10.16).

IEC, 2009. IEC 61400-3: Wind Turbines–Part 3: Design Requirements for Offshore Wind Turbines. Int. Electrotech. Comm. Geneva.

Kirby, J.T., Dalrymple, R.A., 1986. An approximate model for nonlinear dispersion in monochromatic wave propagation models. Coast. Eng. 9, 545–561. doi:10.1016/0378-3839(86)90003-7

Krokstad, J.R., Solaas, F., 2000. Study of Nonlinear Local Flow. Tenth Int. Offshore Polar Eng. Conf.

Malenica, Š., Molin, B., 1995. Third-harmonic wave diffraction by a vertical cylinder. J. Fluid Mech. 302, 203–229. doi:10.1017/S0022112095004071

Marthinsen, T., Stansberg, C.T., Krokstad, J.R., 1996. On the Ringing Excitation of Circular Cylinders. Presented at the The Sixth International Offshore and Polar Engineering Conference, International Society of Offshore and Polar Engineers.

Natvig, B.J., Teigen, P., 1993. Review Of Hydrodynamic Challenges In Tlp Design. Int. J. Offshore Polar Eng. 3.

Paulsen, B.T., Bredmose, H., Bingham, H.B., Jacobsen, N.G., 2014. Forcing of a bottom-mounted circular cylinder by steep regular water waves at finite depth. J. Fluid Mech. 755, 1–34. doi:10.1017/jfm.2014.386

Peng, Z., Raaijmakers, T., Wellens, P., 2013. Nonlinear Wave Group Impact on a Cylindrical Monopile V001T01A044. doi:10.1115/OMAE2013-10838

Rainey, P.J., Camp, T.R., 2007. Constrained non-linear waves for offshore wind turbine design. J. Phys. Conf. Ser. 75, 12067. doi:10.1088/1742-6596/75/1/012067

Rainey, R.C.T., 2007. Weak or strong nonlinearity: the vital issue. J. Eng. Math. 58, 229–249. doi:10.1007/s10665-006-9126-2

Rainey, R.C.T., Chaplin, J.R., 2003. Wave Breaking and Cavitation Around a Vertical Cylinder: Experiments and Linear Theory, in: 18th IWWWFB.

Rienecker, M.M., Fenton, J.D., 1981. A Fourier approximation method for steady water waves. J. Fluid Mech. 104, 119–137. doi:10.1017/S0022112081002851

Sarpkaya, T., 2010. Wave forces on offshore structures. Cambridge University Press.

Sarpkaya, T., 1979. Wave Impact Loads on Cylinders.

Schäffer, H.A., 1996. Second-order wavemaker theory for irregular waves. Ocean Eng. 23, 47–88. doi:10.1016/0029-8018(95)00013-B

Schløer, S., Bredmose, H., Bingham, H.B., 2016. The influence of fully nonlinear wave forces on aero-hydro-elastic calculations of monopile wind turbines. Mar. Struct. 50, 162–188. doi:10.1016/j.marstruc.2016.06.004

Shirzadeh, R., Weijtjens, W., Guillaume, P., Devriendt, C., 2015. The dynamics of an offshore wind turbine in parked conditions: a comparison between simulations and measurements. Wind Energy 18, 1685–1702. doi:10.1002/we.1781

Stansberg, C.T., 2011. Characteristics of Steep Second-Order Random Waves in Finite and Shallow Water 859–869. doi:10.1115/OMAE2011-50219

Stansberg, C.T., Huse, E., Krokstad, J.R., Lehn, E., 1995. Experimental Study of Non-Linear Loads On Vertical Cylinders In Steep Random Waves. Presented at the The Fifth International Offshore and Polar Engineering Conference, International Society of Offshore and Polar Engineers.

Suja-Thauvin, L., Eliassen, L., Krokstad, J., 2014. The scalability of loads on large diameter monopile offshore wind support structures. Presented at the International Wind Engineering Conference, Hannover.

Suja-Thauvin, L., Krokstad, J.R., 2016. Simplified Bottom Fixed Offshore Wind Turbine in Extreme Sea States. Presented at the The 26th International Ocean and Polar Engineering Conference, International Society of Offshore and Polar Engineers, Rhodos (Greece).

Suja-Thauvin, L., Krokstad, J.R., Frimann-Dahl, J., 2016. Maximum loads on a one degree of freedom model-scale offshore wind turbine. Energy Procedia, EERA DeepWind’ 2016, 13th Deep Sea Offshore Wind R&D Conference.

Welch, S., Levi, C., Fontaine, E., Tulin, M.P., others, 1999. Experimental Study of the Ringing Response of a Vertical Cylinder in Breaking Wave Groups. Int. J. Offshore Polar Eng. 9, 276–282.

Wienke, J., Oumeraci, H., 2005. Breaking wave impact force on a vertical and inclined slender pile—theoretical and large-scale model investigations. Coast. Eng. 52, 435–462. doi:10.1016/j.coastaleng.2004.12.008